S. Rathnavel
PG scholar
Department of Aeronautical Engineering
Regional Campus, Anna University
Tirunelveli
India

Dipankar Das
Scientist /Engineer 'SG'
Head, ARD Division, Aero Entity, VSSC
Trivandrum, Kerala
India

J. Bruce Ralphin Rose
Assistant Professor
Department of Aeronautical Engineering
Regional Campus, Anna University
Tirunelveli
India

K. Haroon Rasheed
Scientist /Engineer 'SD'
ARD Division, Aero Entity, VSSC
Trivandrum, Kerala
India

Numerical Simulation Over a Multi-body Launch Vehicle Module at Various Transonic Mach Numbers

Simulations have been carried out for a multi-body launch vehicle configuration using CFD code "PARAS-3D". PARAS-3D is a Reynolds Averaged Navier Stokes equations (RANS) solver with k-ε turbulence model. The transonic regime is a critical regime for any launch vehicle configuration because of its typical aerodynamic characteristics such as shock wave disturbances. CFD flow simulations are done at zero degree angle of attack for various strap-on nose cone angle, nose radius and Mach numbers 0.8, 0.9, 0.95, 1.05. For different positions of strap-on obtained through forward and backward shift from its original position, the influence of strap-on on fore body of the core of launch vehicle is investigated. In this article, the results pertaining to the pressure distribution and Mach contour over launch vehicle configuration is presented.

Keywords: *Launch vehicle, CFD simulation, Strap-on Boosters, Transonic Flow, Turbulent Flow*

1. INTRODUCTION

Launch vehicles are used for delivering payloads to a specified altitude at the proper orbital velocity. The usual values of orbital velocity are extreme one to be achieved by a single stage launch vehicle. Hence, the multi-body launch vehicles are used as an alternative and the addition of strap-on boosters causes problem in aerodynamics part of the launch vehicles [1]. The launch vehicle has to move from subsonic to supersonic regime through Transonic Mach numbers. The aerodynamics of a launch vehicle in the transonic regime is significant because of its complex flow features that include unsteady pressure loads on the fore body of the core vehicle [2]. Therefore, understanding of the physical phenomenon in the Transonic range is ultimately important for the assessment of aerodynamic characteristics of launch vehicle [3,4]. Arash Naghib-Lahouti et al [4] studied about the influence of variable strap-on radius on the performance of the launch vehicle by considering the axial forces only. Wang et al [5] did the supersonic flow field simulations over single and multi-body launch vehicle configurations to compute the pressure distribution around the vehicles. In the same way, Enda Dimitri et al [6] obtained the typical pressure distribution over a vehicle for viscous, turbulent and inviscid cases.

From the previous investigations, it is observed that the aerodynamic data generation and analysis of the launch vehicle is being employed by means of the following methods:

1. Engineering / Analytical tools,
2. CFD Codes,
3. Wind tunnel testing.

In the present work, influence of various slanted strap-on booster nose cone angle and its radius and change in position of strap-on on the fore body of launch vehicle is considered. Navier-Stokes (NS) turbulent solver is used and turbulence is modeled by k-ε model. The flow phenomena such as shock waves, pressure distribution over a launch vehicle are investigated.

2. MATHEMATICAL FORMULATION

The 3-D fluid flow is governed by 3-D Navier Stokes (NS) equations which comprises of continuity, momentum and energy equations. The integral formulations of the three conservation equations are given below. This equation represents the integral form of the continuity equation, which is based on the law of mass conservation.

$$\frac{\partial}{\partial t}\int_{\Omega}\rho d\Omega+\oint_{\partial\Omega}\rho\left(\vec{v}.\vec{n}\right)ds=0 \tag{1}$$

where, ρ is the density of fluid, $\vec{v}$ is the velocity, $\vec{n}$ is the unit normal vector, dS is the elemental surface area and Ω is the control volume.

The expression for the momentum conservation inside an arbitrary control volume Ω which is fixed in space is given by

$$\frac{\partial}{\partial t}\int_{\Omega}\rho\vec{v}d\Omega+\oint_{\partial\Omega}\rho\vec{v}\left(\vec{v}.\vec{n}\right)ds=\int_{\Omega}\rho\overline{f_e}\,d\Omega-\oint_{\partial\Omega}\rho\vec{n}dV+\oint_{\partial\Omega}\overline{\overline{\tau}}.\vec{n} \tag{2}$$

where $\overline{f_e}$ is the body force term, $\overline{\overline{\tau}}$ is the viscous stress tensor.

Received: July 2016, Accepted: August 2016
Assistant Professor, J.Bruce Ralphin Rose, M.E., Ph.D.,
Anna University: Tirunelveli Region, Department of Aeronautical Engineering, India,
E-mail:bruce@auttvl.ac.in
doi:10.5937/fmet1701009R
© Faculty of Mechanical Engineering, Belgrade. All rights reserved

The energy conservation equation is given below.

$$\frac{\partial}{\partial t}\int_{\Omega}\rho E d\Omega+\oint_{\partial\Omega}\rho H\left(\vec{v}.\vec{n}\right)ds=\oint_{\partial\Omega}k\left(\nabla T.\vec{n}\right)ds+\int_{\Omega}\left(\rho\vec{fe}.\vec{v}+\dot{q}_h\right)d\Omega+\oint_{\partial\Omega}\left(\bar{\bar{\tau}}.\vec{v}\right).\vec{n}ds \quad (3)$$

where, H is the total enthalpy, E is the total energy per unit mass, k is the thermal diffusivity coefficient, T is the absolute temperature and $\dot{q}_h$ is the heat transfer per unit mass.

Finite volume formulation is given in the integral form to solve the equation with PARAS [7] as follows,

$$\frac{\partial}{\partial t}\int_{\Omega}Ud\Omega+\oint\left(F_c-F_v\right)ds=Q_T \quad (4)$$

where U is the vector of conserved variables, F is the flux vector function and Q_T is the heat flux. F_c, F_v, U and Q_T are given by,

$$F_c=\begin{bmatrix}\rho HV\\ \rho uV+n_xP\\ \rho vV+n_yP\\ \rho wV+n_zP\\ \rho V\\ \rho kV\\ \rho\varepsilon V\\ \rho zV\end{bmatrix}\quad F_v=\begin{bmatrix}\\ n_x\theta_x+n_y\theta_y+n_z\theta_z\\ n_x\tau_{xx}+n_y\tau_{xy}+n_z\tau_{xz}\\ n_x\tau_{yx}+n_y\tau_{yy}+n_z\tau_{yz}\\ n_x\tau_{zx}+n_y\tau_{zy}+n_z\tau_{zz}\\ 0\\ \left(\mu_l+\frac{\mu_t}{\sigma_k}\right)\frac{\partial k}{\partial x_j}\\ \left(\mu_l+\frac{\mu_t}{\sigma_\varepsilon}\right)\frac{\partial\varepsilon}{\partial x_j}\\ \left(\frac{\mu_l}{\sigma_c}+\frac{\mu_t}{pr}\right)z\end{bmatrix}$$

$$U=\begin{bmatrix}\rho E\\ \rho u\\ \rho v\\ \rho w\\ \rho\\ \rho k\\ \rho\varepsilon\\ \rho z\end{bmatrix}\quad Q_T=\begin{bmatrix}0\\ 0\\ 0\\ 0\\ 0\\ P-\rho\varepsilon\\ \left(C_{\varepsilon1}P-C_{\varepsilon2}\rho\varepsilon\right)\frac{\varepsilon}{k}\\ 0\end{bmatrix} \quad (5)$$

The dynamic viscosity is defined as a sum of molecular viscosity (μ_l) and turbulent viscosity. Therefore,

$$\mu=\mu_l+\mu_t \quad (6)$$

The molecular viscosity μ_l depends on the gas model and this code provides the following viscosity options,

1. Constant viscosity
2. Variations with temperature
   i. Sutherland law
   ii. Power law relation

Now, $$\mu_l=\mu_{ref}\left(\frac{T}{T_{ref}}\right)^{1.5}\left(\frac{T+S}{T_{ref}+S}\right) \quad (7)$$

where C, μ_{ref}, T_{ref} and S are known quantities for the given gas. Hence, Turbulence Viscosity is given by,

$$\mu_t=\frac{c\mu\rho k^2}{\varepsilon} \quad (8)$$

The local viscosity of the flow μ is taken as a sum of the laminar and turbulent viscosities. Hence, the turbulent viscosity is calculated from the K-ε turbulence model [8].

3. GRIDS AND COMPUTATIONAL DOMAIN

Flow simulation over the launch vehicle is done using PARAS 3D tool that practices the Adaptive Cartesian grid. The grid points are highly clustered adjacent to the launch vehicle model to capture the flow field accurately [11]. In adaptive grids the grid moves closer to higher gradient of flow field variables automatically when the iterations begin to start. The grids are further refined until the results are comparatively the same in the criteria for mesh refinement. The solution domain [12] chosen for the present simulation is having the following dimensions.

Upstream ± 14D
Top and Lateral ± 14D

where, (D = Characteristic Diameter). The grid details and grid refinement levels are mentioned in Table 1 and Table 2 respectively.

Table 1. Grid Refinement Level

Base grid level	3
Curve /grid refinement level	4
Max refinement level	4
Flow refinement level	1

Table 2. Grid Details

Type	Cartesian Grid
Total no of cells	25813746
Grid Refine criterion	0.01
Grid unrefined criterion	0.01

The flow boundary assumptions relevant to the X, Y and Z directions are listed as follows,

At X minimum condition: Inflow conditions
At X maximum condition: Subsonic flow condition
At Y minimum condition: Subsonic flow condition
At Y maximum condition: Subsonic flow condition
At Z minimum condition: Subsonic flow condition
At Z maximum condition: Subsonic flow condition

The meshed view of the launch vehicle model is presented in Figure 1(a). Additionally, the finest mesh view adjacent to the vehicle boundary is presented in Figure 1 (b). The first cell size is assumed to be 1 mm

against the base level grid while it is fixed at 6 in the meshing process. Instead of grid independency studies, a flow refinement process is done in the range of 4 (Min.) to 8 (Max.) flow refinement levels. In the present study, for example if the difference in pressure gradient is 0.01 between the two adjacent cells, then the solution refinement process will be initialized according to the defined flow refinement criterion. Subsequently, the flow refinement criterion is fixed at 0.01 and the numerical computations are done at the Angle of Attack (AoA) α = 00. The operating altitude is assumed about 4.95 km from the mean sea level.

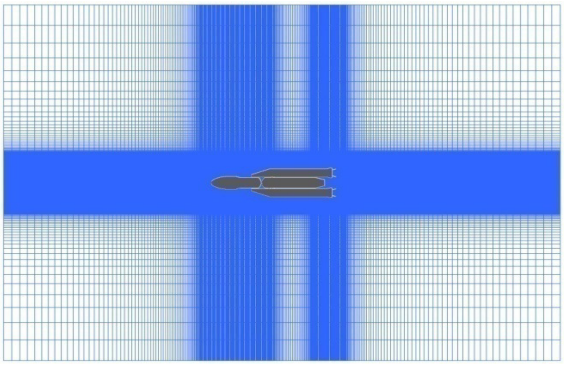

(a). Full scale meshed view of the model

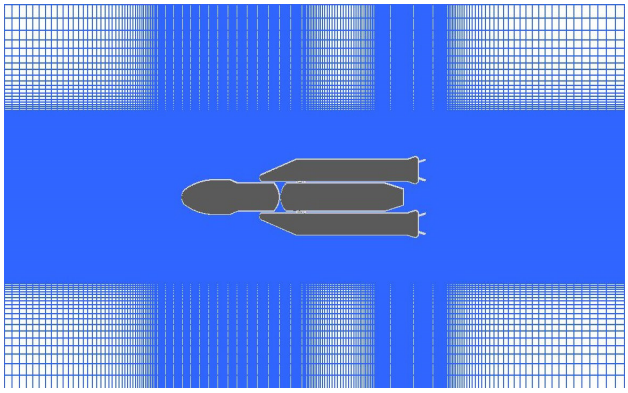

(b). Finest mesh view adjacent to the vehicle boundary

Figure 1. Meshed model of launch vehicle

4. RESULTS AND DISCUSSION

4.1 Effects of various slanted strap-on nose radius on the launch vehicle Pressure coefficient

To investigate the influence of slanted strap-on nose radius (R_N) on the pressure distribution over fore body of launch vehicle, the radius is varied from 0.5 m, 0.7 m 1.0 m at constant nose cone angle 20^0 and 25^0 respectively. The AoA for the numerical computation is assumed as $\alpha = 0^0$. Simulations have been carried out at two transonic Mach numbers (M = 0.8 & M = 0.9) using PARAS-3D to compute the C_p distributions [10].

Figure 2 shows the variation of C_p along X/L Direction at slanted nose cone angle 20^0 with various nose radius values at M = 0.8 and M = 0.9. Initial peak in C_p falls down rapidly and there is a slight compression because of the slope of the geometry. C_p decreases gradually over the nose of the heat shield and on the fore body cylinder C_p increases due to the presence of transonic shock at M = 0.9. It is also observed that there is no great difference in C_p till the end of the cylinder boat tail junction (i.e)., fore body of cylinder) for various nose radius magnitudes. At 20^0 slanted nose cone angle with increase in nose radius, C_p changes adjacent to the fore body of the launch vehicle. At higher nose radius of fore body cylinder and boat tail region, C_p decreases because of the strength of the expansion waves and also sequentially the total axial force coefficient increases.

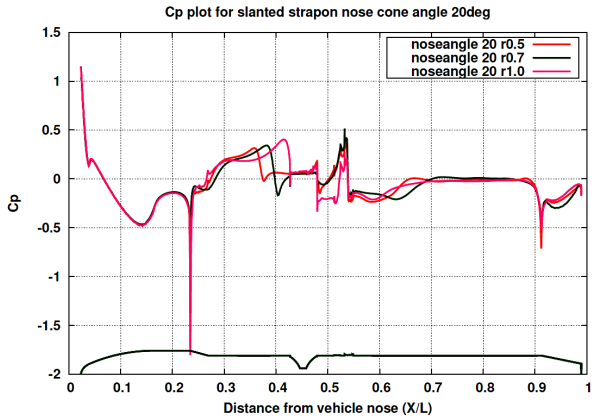

(a). Variation of C_p at M = 0.8

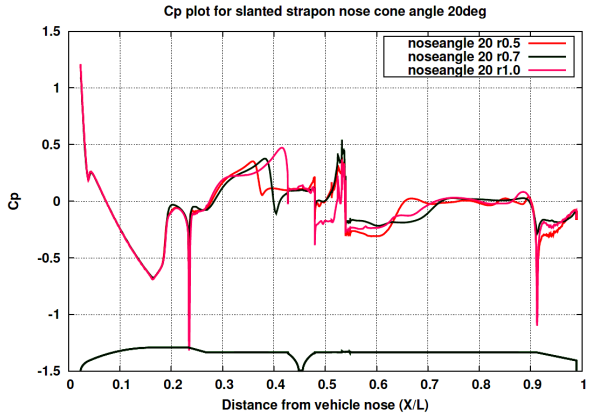

(b). Variation of C_p at M = 0.9

Figure 2. Variation of C_p along X/L direction for slanted nose cone angle 20^0 with various nose radius at M = 0.8 and M = 0.9

The upstream influence of higher strap-on nose radius intensifies the C_p at the fore body of launch vehicle. The Mach palette of launch vehicle for $\theta_N = 20^0$ & R_N = 0.5 m, 0.7 m, 1.0 m respectively at M = 0.9 is presented in Figure 3. From the captured flow phenomenon, the Mach palettes are observed in the range between M = 0.8 to M = 1.19 in the transonic regime. The flow stagnates at the nose of heat shield followed by an expansion of the flow over the ogive region. Moreover, flow tries to recover over the cylindrical region on the heat shield, and at the cylinder boat-tail junction it expands on the fore body of launch vehicle. Because of an increase in the R_N, the strength of appeared expansion wave rises [1] at the cylinder boat-tail as displayed in Figure 3.

The variation of C_p along the distance from the vehicle nose (X/L) at slanted nose cone angle about 25^0 with various nose radius at M = 0.8 and M = 0.9 are highlighted in Figure 4. At 25^0 slanted nose cone angle

with increase in nose radius, greater C_p difference is observed from the boat tail region as compared with the previous case. The strength of expansion waves increases at the end of heat shield region at high Mach numbers and at the mid portion of vehicle a greater influence is observed closer to strap-on nose cone.

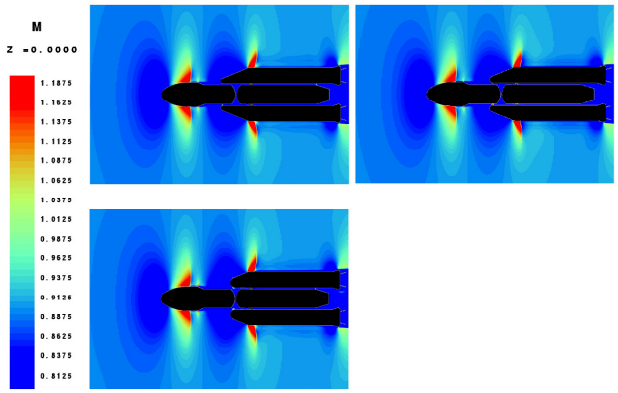

Figure 3. Mach palette of launch vehicle for θ_N = 20^0 & R_N = 0.5 m, 0.7 m, 1.0 m at M = 0.9

The upstream influence of R_N on the fore body of launch vehicle increases for additional nose radius. For 25^0 slanted strap-on nose cone angle, the Mach number trends caused by the added nose radius, are displayed in Figure 5.

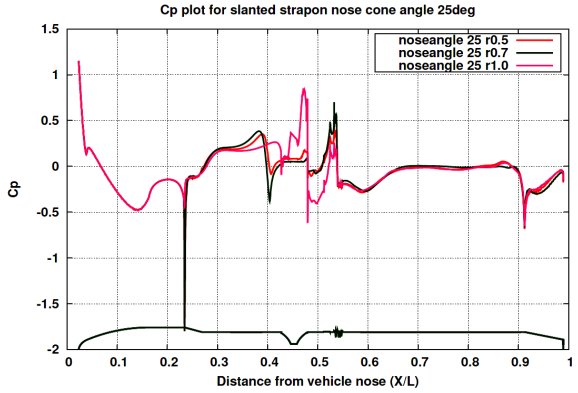

(a). Variation of C_p at M = 0.8

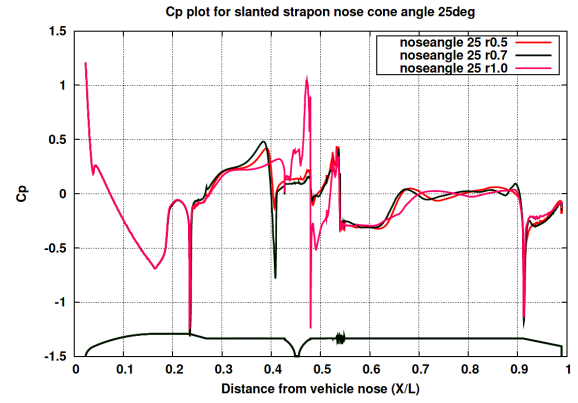

(b). Variation of C_p at M = 0.9

Figure 4. Variation of C_p along X/L direction for slanted nose cone angle 25^0 with various nose radius at M = 0.8 and M = 0.9

At transonic Mach numbers, the characteristic wave travels in all directions and there is an upstream influence of the strap-on on the fore body of launch vehicle. It is also quantified that for higher R_N the total axial force coefficient increases and it induces more upstream effects on the flow over fore body of the launch vehicle [4].

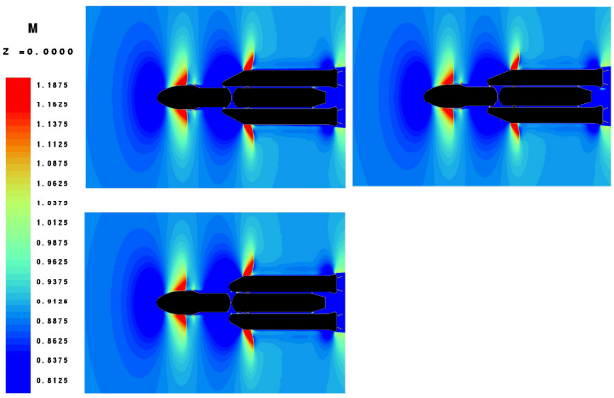

Figure 5. Mach palette of launch vehicle for θ_N = 25°& R_N = 0.5 m, 0.7 m, 1.0 m at M = 0.9

4.2 Effects of change in position of strap-on on the fore body of launch vehicle

Strap-on of the straight nose cone is used for the flow simulations to investigate the effects of their position on the launch vehicle at various transonic Mach numbers (M = 0.8, 0.9, 0.95, and M = 1.05) using PARAS-3D. In the present study, the effect of change in position of strap-on on the fore body of launch vehicle is observed by moving the strap-on position forward and backward for about 2 m and 4 m respectively. Because of the forward and backward movements of the strap-on, the Cp distribution will be modified significantly as compared to its original position. The variation of Cp distribution with respect to X/L Direction for different strap-on positions at M = 0.8 and M = 0.9 are shown in Figure 6. Initial peak magnitude of CP falls down to approximately zero because of the flow expansion over nose cap region. At the nose cap-cone junction, the flow is compressed due to the shape of geometry. The Cp is not varying till cone-cylinder junction on the fore body of launch vehicle at different positions of strap-on at transonic Mach numbers. The pressure oscillations along the body from X/L = 0.5 to X/L = 0.65 take place because of the formation of shock waves near the core of launch vehicle hits the strap-on nose cone. As the strap-on position is moved, the location of pressure oscillations is also moving significantly. Moreover, it depends upon the order of accuracy of the numerical scheme implemented for the analysis.

In the heat shield region, Cp is reasonably higher for the case of 4 m forward shifting of strap-on. Cp is approximately same for 2 m forward and 2 m backward shifting of strap-on that is higher as compared with the initial position of strap-on. On the other hand, for 4 m backward shift case Cp is almost equivalent as its original position of strap-on. Hence, the different position (X/L) of strap-on increases the upstream influence of Cp except 4 m backward shift of strap-on compared with its original position at M = 0.8. When M = 0.9, near the heat shield region, upstream influence of

2 m and 4 m forward shift of strap-on is higher and as a result Cp increases. For the backward shift of strap-on, Cp remains the same for 2 m shift and Cp is reduced for 4 m shift as compared to the initial position at M = 0.9.

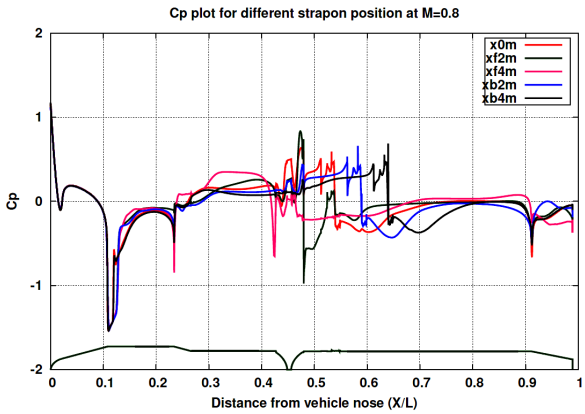

(a). Variation of C_p at M = 0.8

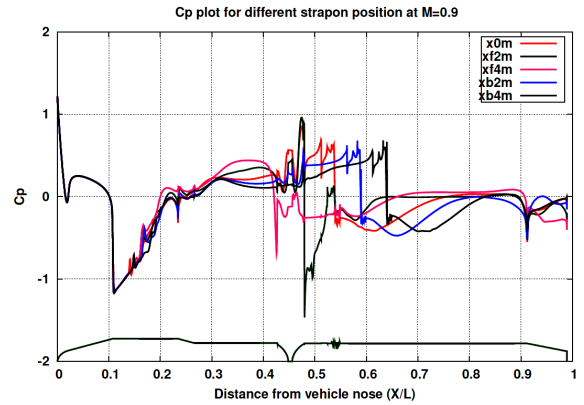

(b). Variation of C_p at M = 0.9

Figure 6. Variation of C_p along X/L direction for different position of strap-on at M = 0.8 and M = 0.9

The C_p distribution along X/L direction of the launch vehicle for different strap-on position at M = 0.95 and M = 1.05 are presented in Figure 7. In the PARAS-3D CFD code, pressure boundary condition is given to solve the problem. Meaning of pressure at this point in the CFD code is "Pressure boundary condition that is meant for subsonic outflow situations. The user can specify pressure and its value imposed on the boundary. Here, the Primitive variable for Riemann solver is applied with the exception that p* value is imposed as the applied pressure. In case, if the flow becomes supersonic with pressure boundary, then it will be treated as a shift in the boundary condition.

As the Mach number reaches about M = 0.95 and M = 1.05, in the heat shield region because of the forward 2m & 4m shifts of strap-on Cp increases. However, Cp is almost similar for 2 m backward shift and it decreases further for 4 m backward shift as compared with the original strap-on position. Hence, there is higher upstream influence on the fore body cylinder for forward of strap-on and the influence is less for backward shift of strap-on. Consequently, higher influence is observed in the mid part of the launch vehicle closer to the nose of strap-on [9].

As the Mach number increases, transonic shock wave moves aft/backward of the fore body of launch vehicle. Figure 8 and 9 show Mach palettes of launch vehicle for different positions of strap-on at M = 0.95. Because of the forward shift of strap-on there is an upstream influence on fore body of cylinder increases, which reduces the turning angle of expansion wave forward compared to its original position of strap-on. For downward shift of strap-on, the influence of pressure loads on fore body of launch vehicle is reduced, which increases the turning angle of an expansion wave further backward compared to its original position of strap-on.

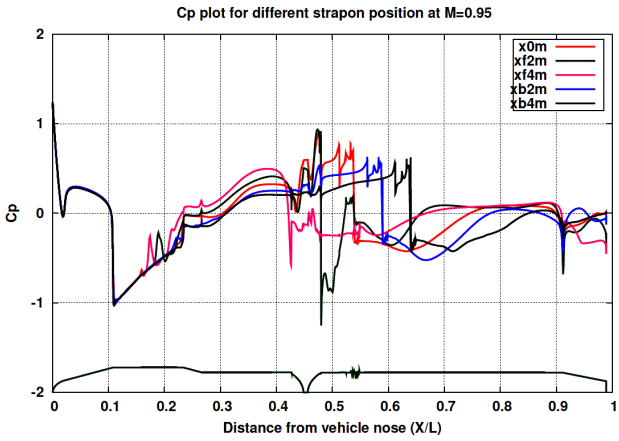

(a). Variation of C_p at M = 0.95

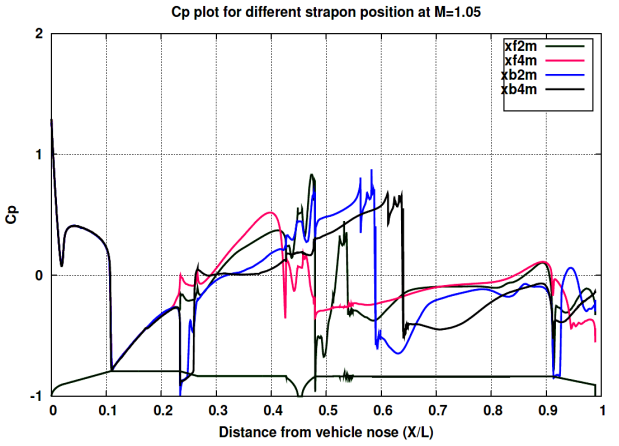

(b). Variation of C_p at M = 1.05

Figure 7. Variation of C_p along X/L Direction for different position of strap-on at M = 0.95 and M = 1.05

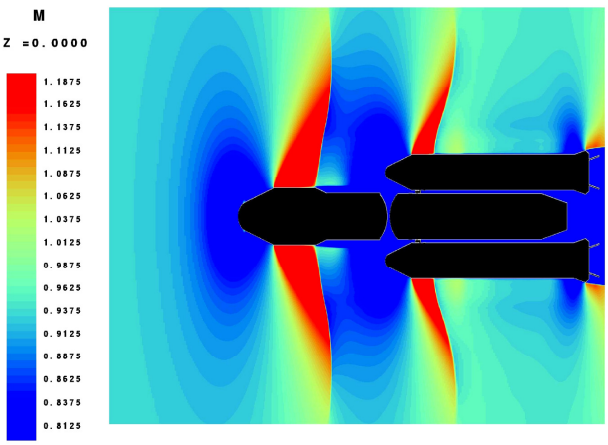

Figure 8. Mach palettes of launch vehicle for initial position of strap-on at M = 0.95

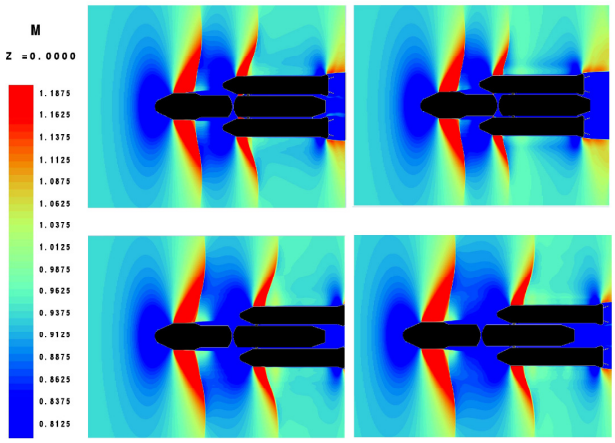

Figure 9. Mach palettes of launch vehicle for 2 m, 4 m forward and backward shift of strap-on at M = 0.95

5. CONCLUSIONS

Numerical simulations are done for a launch vehicle in the transonic regime to compute the associated complex flow field, aerodynamic characteristics over the vehicle and the effect of the strap-on nose cone on the fore body pressure distributions. Significant observations are made in the course of analysis to customize the transonic flow properties around the vehicle. For higher strap-on nose cone angle and nose radius, the influence of aerodynamic characteristics on the fore body of launch vehicle is not significant although moderate influence is observed in the mid part of the vehicle closer to strap-on nose cone. If the strap-on is moved forward, then the influence near fore body of launch vehicle is great but if the strap-on is moved backward, then the influence adjacent to fore body of launch vehicle is less as compared to its original position.

REFERENCES

[1] Pankaj Priyadarshi and Dipankar Das (2003), 'Launch Vehicle Aerodynamics', Proceedings of Symposium on Applied Aerodynamics and Design of Aerospace Vehicles, SAROD-2003, Bangalore, India.

[2] S.Parameshwari, G.Vidya, K.Manokaran, J. Bruce Ralphin Rose (2013), 'CFD simulation of flow over a multi body launch vehicle at transonic and supersonic Mach numbers', INCAM, IIT Madras.

[3] Ana Cristina Avelar, Edson Basso, Joao Batista Filho, Pedro Geo vanny Martinez Romero, Jessica Jia Ling Hsu (2014), 'Experimental and Numerical analysis of the flow patterns around a sounding rocket in the transonic regime', AIAA2014-3136.

[4] Arash Naghib-Lahouti, Amir Nejat and Taravat Khadivi (2002), 'Parametric Analysis of Aerodynamic Characteristics of Launch Vehicles with strap-on boosters', ICAS2002 CONGRESS.

[5] J.C.T.Wang, P.T.Than, G.F.Widhopf (1991), 'Multi-Body Launch Vehicle Flow field Simulation', AIAA-91-0072.

[6] Enda Dimitri V.Bigarella, and Joao Luiz F.Azevedo (2005), 'Numerical Study of Turbulent Flow over Launch Vehicle Configurations', Journal of Spacecraft, Vol. 42, pp 266-276.

[7] 'PARAS-3D user's manual', Vikram Sarabhai Space Centre, (2011), India.

[8] Vinod Kumar and Dipankar Das, 'Numerical Simulation of flow over a rocket Body using PARAS-3D', Vikram Sarabhai Space Centre, MS 202, pp 1-17.

[9] M. Mani, A. Naghib-Lahouti and M. Nazarinia (2004), 'Experimental and numerical aerodynamic analysis of a satellite launch vehicle with strap-on boosters, The Aeronautical Journal, paper no 2885.

[10] Enda Dimitri Viera Bigarella, Edson Basso and Joao Luiz F. Azevedo (2003), 'Multigrid Adaptive-Mesh Turbulent Simulations of Launch Vehicle Flows', AIAA 2003-4076.

[11] Enda Dimitri Vieira Bigarella, Joao Luiz F. Azevedo and Leonardo Costa Scalabrin (2007), 'Centered and Upwind Multigrid Turbulent Flow Simulations of Launch Vehicle Configurations', Journal of Spacecraft, Vol. 44, pp 52-65.

[12] R.C.Mehta (1997), 'Transonic Flow Simulation for a Bulbous Heat Shield', Journal of Spacecraft, Vol 34, pp 561-564.

NOMENCLATURE

PARAS	Parallel Aerodynamic Simulator
CFD	Computational Fluid Dynamics
CF	Convergence Factor
C_p	Pressure coefficient
α	Angle of attack
M	Free Stream Mach number
ρ	Density
θ_N	Strap-on Nose Angle
R_N	Strap-on Nose Radius
u,v,w	Velocity components in x, y and z directions
μ	Viscosity coefficient
P	Pressure
e	Total internal energy
k	Thermal conductivity
T	Temperature
τ	Shear stress
γ	Ratio of specific heats
F	Flux vector function
$\vec{v}$	Velocity of the vector
$\vec{n}$	Unit normal vector
dS	Elemental surface area
Ω	Control volume
$\overrightarrow{f_e}$	Body force
$\overline{\overline{\tau}}$	Viscous stress tensor
H	Total enthalpy
E	Total energy per unit mass
$\dot{q}_h$	Heat transfer per unit mass
U	Vector of conserved variables
Q_T	Heat flux
μ_l	Molecular viscosity

μ_t	Turbulent viscosity
n_x, n_y, n_z	Flux vector in x y and z directions

НУМЕРИЧКА СИМУЛАЦИЈА ИЗВЕДЕНА НА МОДУЛУ ВИШЕСТЕПЕНЕ РАКЕТЕ ПРИ РАЗЛИЧИТИМ ВРЕДНОСТИМА МАХОВОГ БРОЈА

С. Ратнавел, Д. Дас, Ј. Б. Р. Роуз, К. Х. Рашид

Симулација је изведена на конфигурацији вишестепене ракете применом ЦФД кода „Парас-3Д“. „Парас-3Д“ је РАНС солвер са *κ-ε* моделом турбуленције. Трансонични режим је од највећег значаја за сваку конфигурацију ракете због њених типичних аеродинамичких карактеристика као што је поремећај ударног таласа. ЦФД симулације кретања су вршене при нултом нападном углу за различите углове strap-on мотора на носном конусу, радијуса носног дела и вредности Маховог броја 0,8; 0,9; 0,95 и 1,05.

За различите положаје strap-on мотора добијене кретањем напред и назад из првобитног положаја, истражује се утицај strap-on мотора на предњи део средњег дела ракете. У раду су приказани резултати дистрибуције притиска и промене вредности Маховог броја по целој конфигурацији ракете.